Journal of Innovative Optical Health Sciences
Vol. 2, No. 4 (2009) 431–440

World Scientific
www.worldscientific.com

APPLICATION OF DOPPLER OPTICAL COHERENCE TOMOGRAPHY IN RHEOLOGICAL STUDIES: BLOOD FLOW AND VESSELS MECHANICAL PROPERTIES EVALUATION

MARCO BONESI[*,§,¶], ANEURIN J. KENNERLEY[†,‖], IGOR MEGLINSKI[‡,**] and STEPHEN MATCHER[§,††]

[*]*Center for Biomedical Engineering and Physics*
Medical University of Vienna
Währinger Strasse 13, 1090, Vienna, Austria

[†]*Department of Psychology, University of Sheffield*
Sheffield, S10 2TN, UK

[‡]*Department of Physics, University of Otago*
Dunedin 9054, New Zealand

[§]*Department of Engineering Materials*
University of Sheffield, Sheffield, S3 7HQ, UK

[¶]*marco.bonesi@meduniwien.ac.at*
[‖]*a.j.kennerley@sheffield.ac.uk*
[**]*igor@physics.otago.ac.nz*
[††]*s.j.matcher@sheffield.ac.uk*

Doppler Optical Coherence Tomography (DOCT) is a noninvasive optical diagnostic technique, which is well suited for the quantitative mapping of microflow velocity profiles and the analysis of flow-vessel interactions. The noninvasive imaging and quantitative analysis of blood flow in the complex-structured vascular bed is required in many biomedical applications, including those where the determination of mechanical properties of vessels or the knowledge of the mechanic interactions between the flow and the housing medium plays a key role. The change of microvessel wall elasticity could be a potential indicator of cardiovascular disease at the very early stage, whilst monitoring the blood flow dynamics and associated temporal and spatial variations in vessel's wall shear stress could help predicting the possible rupture of atherosclerotic plaques. The results of feasibility studies of application of DOCT for the evaluation of mechanical properties of elastic vessel model are presented. The technique has also been applied for imaging of sub-cranial rat blood flow *in vivo*.

Keywords: Optical imaging; optical coherence tomography; Doppler OCT; blood flow; elastic vessels; mechanical properties.

1. Introduction

Optical Coherence Tomography (OCT) is a well established optical diagnostic modality, widely used for the imaging of internal microstructure of various composite materials[1,2] and biological tissues.[3] The technique provides high resolution (up to 1–15 μm) cross-sectional images from sample depths of up to 1–1.5 mm.[4–6] OCT imaging can be performed *in situ*, noninvasively and in real time (several frames per second for 200–500 pixel images).[7,8] The unique features of this technology enable a broad range of research and clinical applications.[9–12] OCT has been interfaced with a wide range of imaging delivery systems[13] and probes.[14,15] OCT also has many applications in flow-related biomedical studies, e.g. to differentiate plaque constituents *ex vivo* and *in vivo*.[16–20]

Doppler OCT (DOCT) is an extension of conventional OCT in that it has the capability to simultaneously image the sample morphology and the flow/velocity profiles therein.[21–26] DOCT has a resolution about $10\,\mu\text{m} \cdot \text{s}^{-1}$ and has been applied across a number of disciplines. DOCT has been successfully applied to measure parabolic and non-parabolic velocity profiles,[27] local shear rate,[28] and red blood cell (RBC) concentrations *in vitro*.[29] *In vivo*, DOCT applications include feasibility studies describing measurements of blood flow in the subsurface vasculature of laboratory animals,[30–32] subsuperficial human skin vessels,[33] and cutaneous disorders.[16,34,35] In addition DOCT allows the assessment of the retinal blood flow dynamics, which can be used for diagnosis of diabetic retinopathy and glaucoma.[23] DOCT also has potential applications to neuro-imaging; during neuronal activity, an increase in metabolic demand results in local blood flow increases. However, the exact neuro-vascular coupling mechanisms behind this are still an area of intense research. The spatial and temporal resolution of DOCT offers the ability to image the flow and dynamics of single blood vessels and see how the brain regulates the vessel network in the different vascular compartments (arterioles, venuoles, etc.). Such information could be vital for a better understanding of the temporal dynamics of noninvasive imaging techniques such as Blood Oxygenation Level Dependent (BOLD) functional Magnetic Resonance Imaging (fMRI) which are confounded by these hemodynamic variables.

In current paper, we consider application of DOCT for rheological studies. DOCT has the potential of being able to noninvasively determine the local mechanical properties of blood vessels *in vivo*. Such investigations have clinical application as changes in the elastic modulus may provide early warnings of systemic vascular diseases. As a feasibility study, we apply DOCT for the determination of mechanical properties of microvessels. Alternative methods do exist; in large arteries (such as the aorta) the compliance can be noninvasively determined by an indirect method of measuring the pulse wave velocity. However, in sub-mm blood microvessels this is not possible due to the short time interval involved. From the equation of continuity for an incompressible fluid it is possible to indirectly determine the pulse wave velocity by measuring simultaneous changes in the vessel diameter and flow velocity. Preliminary results (blood flow imaging and associated morphological changes) from an artificial elastic vessel model and *in vivo* subcranial rat model are presented.

2. Method and Materials

The flow velocity measurement principle relies on the Doppler effect exhibited by wave phenomena: the apparent change in frequency due to the relative motion between an observer and a source.[36] OCT and DOCT systems are based on the technique of low-coherence gating detection interferometry.[7,8,37] Detailed descriptions of the principles of OCT and DOCT are beyond the scope of this manuscript but can be widely found across the literature.[7,8,37–39] DOCT measurements were performed using a swept-source (SS) commercial OCT system (OCS1300SS, *Thorlabs Ltd.*, UK). The Thorlabs SS-OCT system implemented a 16 KHz SS laser centered at 1300 nm and FWHM of about 150 nm, giving a spatial resolution of $\sim$5 μm in air. Velocity profiles were extracted by applying the phase-resolved DOCT technique, i.e. phase changes measured between sequential axial scans to reconstruct the velocity image from continuation of the analytic signal. The time interval between sequential axial scans is much greater than the acquisition time of an individual pixel, hence reducing the minimum detectable Doppler frequency by several orders of magnitude. The advantage of SS-DOCT with the implemented phase-resolved technique is that the velocity sensitivity is decoupled from the spatial resolution while maintaining a high image acquisition rate.[29]

For a vessel of equilibrium radius R it is straightforward to show that the instantaneous radial expansion $\xi(t)$ and the instantaneous mean flow velocity $\bar{w}(t)$ are related to each other as:

$$\frac{2\xi(t)}{R} = \frac{\bar{w}(t)}{c}, \tag{1}$$

where c is the complex apparent pulse wave velocity. The real part of this velocity is the apparent phase velocity, whereas the imaginary component relates to the attenuation of the wave amplitude with respect to distance. If cyclic oscillations in $\xi(t)$ and $\bar{w}(t)$, induced for example by cardiac oscillations, are simultaneously measured then comparing the complex Fourier amplitudes of these quantities can, in principle, allow a direct measurement of c. In the case of an infinitely long, uniform elastic tube then c can itself be related to the underlying mechanical properties of the vessel and the fluid flowing within it:

$$\frac{1}{c} = \sqrt{D\rho(1-\sigma^2)}\left(1 - \frac{2J_1(\alpha i^{3/2})}{\alpha i^{3/2} J_0(\alpha i^{3/2})}\right)^{-1/2}, \tag{2}$$

where D is the vessel compliance (the fractional increase in cross-sectional area per unit transmural pressure increase), σ is the Poisson's ratio of the vessel wall, ρ is the fluid density, α is the dimensionless "Womersley" parameter $\alpha = R\sqrt{2\pi f\rho/\mu}$, f is the oscillation frequency, μ is the kinematic viscosity of the fluid, and J_0 and J_1 are Bessel functions.

The SS-DOCT system was used to measure flow velocity profiles within artificial elastic vessels and an *in vivo* animal model.

2.1. *Artificial elastic vessels*

Artificial vessels were developed to mimic mechanical properties of human blood microvessels. We tested several materials as artificial elastic vessels, including latex and silicone rubber. The internal diameter ranged from 0.4 to 1.0 mm and the axial extension (length) from 5 to 15 mm. The fabricated vessels were used to access preliminary analysis of the interaction between flow dynamics (typically sinusoidal oscillatory flow) and vessel compliance.

An artificial vessel made from latex is shown in Fig. 1. Vessels were built by dip-coating a syringe needle and then gently separating the rubber sheath from the needle surface. Separation was eased with injection of water through the needle, the pressure of which forced water back between the needle and the rubber. The formed vessel was then

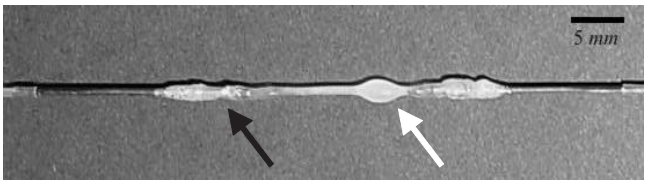

Fig. 1. An example of an artificial vessel used for DOCT measurements. The 10 mm long expandable latex vessel had 0.8 mm relaxed internal diameter. The white arrow indicates a radial expansion of the vessel when liquid is injected. The black arrow indicates the vessel–needle coupling, fixed and covered with cyanoacrylate glue.

coupled with syringe needles on both extremities using cyanoacrylate glue, and the needles coupled to the hydrodynamic system (see Fig. 2). Due to its convenient optical properties for DOCT imaging, 1% stock solution of *Intralipid* 10% in distilled water was used as the flowing liquid during the *in vitro* experiments.

2.2. *Hydrodynamic experimental setup*

The hydrodynamic setup used for the experiments is illustrated in Fig. 2. A mechanical pump consisting of a syringe connected a flexible linkage to the perimeter of a rotating circular cam was used to generate a quasi-sinusoidal flow waveform through the elastic artificial microvessel. The cam rotates at an adjustable frequency (typically 0.5–2 Hz). A rotating frequency of 1 Hz was used in the experiments. The rotary syringe pump was coupled to the inlet of the elastic microvessel via a Y-coupling and the other arm fed an overflow reser-

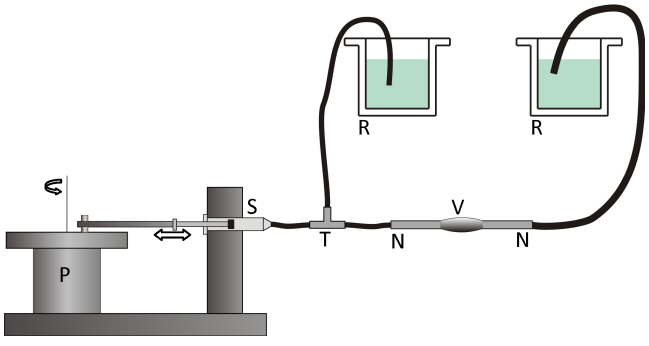

Fig. 2. Schematic representation of the hydrodynamic setup used in the experiments. P — rotary pump; S — syringe, fixed on a metal holder; T — T-shaped adjustable flow constrictor; N — metal gauge (syringe needle); V — artificial elastic microvessel; R — reservoirs, kept at same height above the microvessel. The pump was rotating at 1 Hz, generating a quasi-sinusoidal input volume flow rate profile.

voir. An adjustable flow constrictor between the Y-coupling and the microvessel was used to adjust the overall volume flow rate into the microvessel. The distal end of the microvessel was connected to an identical reservoir. Both reservoirs were maintained at a height of about 20 cm above the height of the microvessel and rotary pump. This generated a static positive transmural pressure difference across the wall of the microvessel, which prevented it from collapsing on the extraction phase of the pump rotation.

2.3. *In vivo animal preparation*

All aspects of these methods and their development were performed with UK Home Office approval under the Animals (Scientific Procedures) Act 1986. We used a female Hooded Lister rat weighing approximately 270 g which was kept in a 12-hour dark/light cycle environment at a temperature of 22°C with food and water *ad libitum*. The animal was anaesthetized with urethane. Rectal temperature was maintained at 37°C throughout surgical and experimental procedures using a homeothermic blanket (Harvard Apparatus). Animals were tracheotomized to allow artificial ventilation and measurement of end-tidal CO_2. Ventilation parameters were adjusted to maintain blood gas measurements and end-tidal CO_2 within physiological limits. The left and right femoral veins and arteries were cannulated and allowed drug infusion and measurement of mean arterial blood pressure, respectively. Phenylephrine (0.13–$0.26\,\mathrm{mg \cdot h^{-1}}$) was infused to maintain blood pressure between physiological limits (MABP, 100–110 mmHg). Animals were placed in a stereotaxic frame (Kopf Instruments). The skull overlying the right somatosensory cortex (an area of brain with unique angio-architecture — see Fig. 5(a)) was thinned to translucency (∼50–100 μm) with a dental drill under constant cooling with saline. DOCT uses a 1,300 nm laser which has a depth penetration through turbid media of 1–1.5 mm. Therefore, the thin cranial window is necessary to reduce optical signal degradation through the skull. This preparation holds one further advantage in that the vascular net can also be visualized for optimum placement of the DOCT laser beam (Fig. 5(a)). A 30 mm diameter Perspex ring was placed around the thin window and secured in place with dental cement. Saline was injected into the formed well leaving a good optical boundary for high resolution imaging of the vessel network prior to DOCT measurements. Once completed the stereotaxic frame was placed under the Thorlabs DOCT microscope. The frame was tilted slightly to induce a Doppler angle between the propagation direction of the probing low coherent laser radiation and the flow velocity vector.

3. Results

3.1. *Artificial vessel*

DOCT has been applied to observe quantitatively the flow dynamics in artificial elastic vessels, and also to characterize mechanical properties of the vessels from the acquired data. To visualize the velocity profiles, a Doppler angle between the propagation direction of the probing low coherent laser radiation and the flow velocity vector (assumed parallel to the sample axis of symmetry) was set to ∼75°.

Flow velocity maps from the elastic latex vessel are shown in Fig. 3. The flow was set in motion by a rotary pump operated at 1 Hz, which generated a quasi-sinusoidal input volume flow rate.

In relation to different velocity intensities during a pumping-withdraw cycle, the expansion of the vessel was quasi-isometric and the flow regime remained laminar for most of the cycles. Figures 3(c), 3(i), and 3(j) present an aliasing in the velocity data, due to the fact that the peak velocity was higher than the detection range of the measuring device.

Figure 4 shows the results of the DOCT measurements of axial flow speed and vessel diameter as a time series and also the corresponding Fourier amplitude spectra. From the complex amplitude spectra we can extract the complex quantity $\tilde{\xi}(f)/\bar{w}(f) = 0.5R/c$ which for this data set is measured as $0.0015 \cdot \exp(-0.22i)$. Hence for the vessel of equilibrium radius 400 microns we can infer $1/c = 7.5\exp(-0.22i)\,\mathrm{s \cdot m^{-1}}$. In comparison, the previous equation predicts that for a vessel of compliance $6.1 \times 10^{-5}\,\mathrm{m^2 \cdot N^{-1}}$ containing fluid of density $1{,}000\,\mathrm{kg \cdot m^{-3}}$ then $1/c_0 = 0.25\,\mathrm{s \cdot m^{-1}}$. For the vessel radius of 400 microns, $f = 1\,\mathrm{Hz}$, $\mu = 10^{-3}\,\mathrm{N \cdot s \cdot m^{-2}}$ and $\sigma = 0.5$ we have $\alpha = 1.0$ and Eq. (2) predicts $1/c = 2.3 \cdot \exp(-0.72i)/c_0 = 0.58 \cdot \exp(-0.72i)\,\mathrm{s \cdot m^{-1}}$. There is, thus, a noticeable discrepancy between the measured and expected pulse wave velocities.

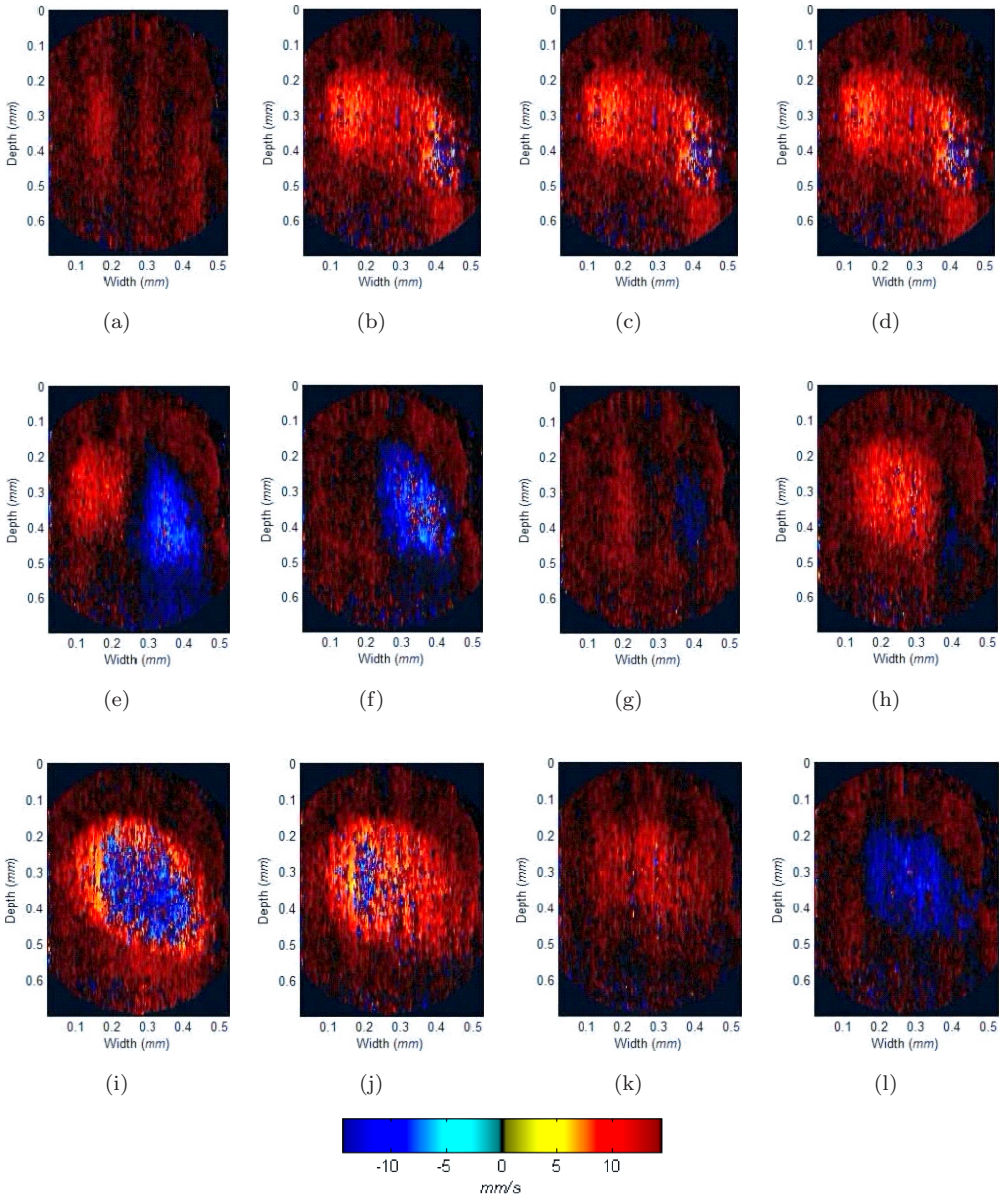

Fig. 3. The dynamics of flow in the artificial elastic vessel (latex) under quasi-sinusoidal inlet volume flow rate regime. From (a) to (l) are shown the cross-sectional flow velocity profile. The measurements are produced at the fixed position in the vessel during one oscillatory cycle (about 1 Hz). The velocity amplitude is color-coded, red indicating flow moving away from the pump, blue indicating flow moving towards the pump. The vessel internal diameter at rest was ∼0.5 mm; the image dimensions are 0.5 mm × 0.7 mm.

3.2. *In vivo measurements*

We investigated the possibility of determining the mechanical properties of blood microvessels and cerebral blood flow (CBF) from the rat model *in vivo*.

Figure 5(a) shows a high resolution image of the cerebral vascular net; the middle cerebral artery (red) and venous drainage system (blue) are highlighted; the arrow indicates the site and direction from which DOCT tomograms were acquired. Figure 5(b) shows the Doppler data, the arrows pointing to detected vessels. A time series of normalized Doppler data was taken through V_a (see Fig. 5(c)). Power spectrum analysis of the time series showed a 0.15 Hz oscillation in the data. Such physiological oscillations were first recorded with laser Doppler flowmetry.[40]

It was believed to only be an oscillation in blood flow, however, Mayhew *et al.*[41] using intrinsic optical imaging showed similar oscillations in changes in total blood volume in the anaesthetized animal

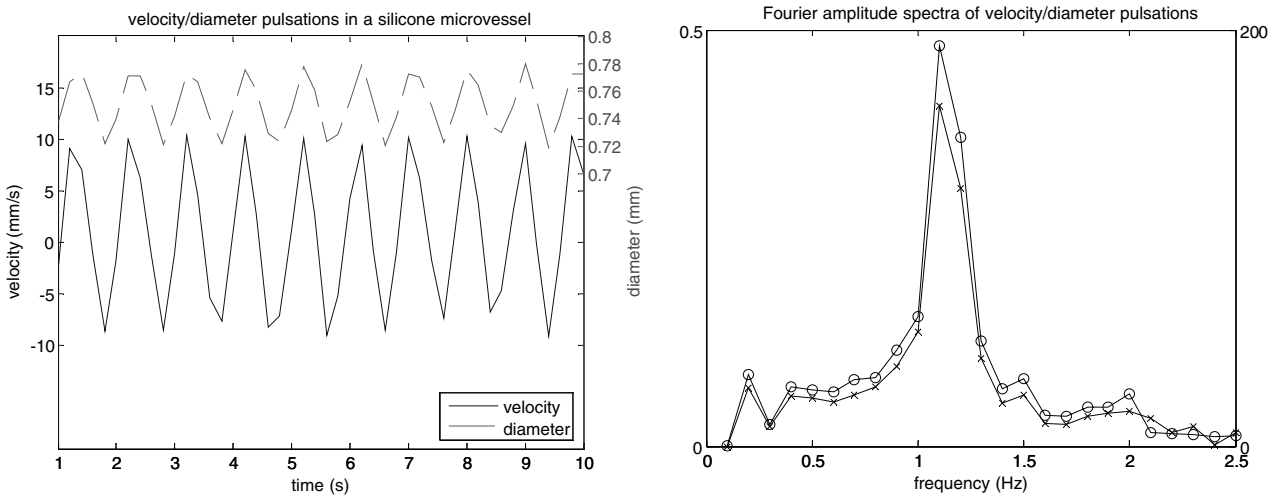

(a) (b)

Fig. 4. Experimental results. (a) Instantaneous mean flow velocity (solid curve) variations vs related instantaneous vessel radius (dotted curve) changes at 1 Hz oscillatory flow. (b) Computed Fourier amplitude spectra of flow velocity data (dots) vs vessel radius data (crosses).

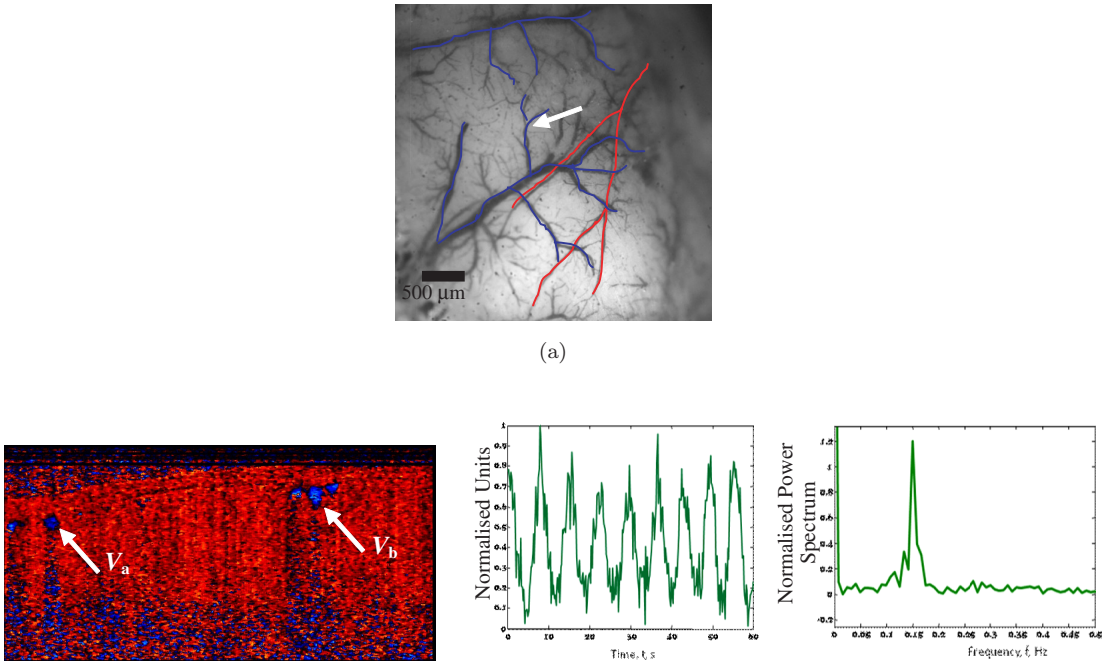

(a) (b) (c)

Fig. 5. *In vivo* measurements of subcranial cerebral blood flow of a rat. Top-view photography of the rat blood vessels net. (a) The arrow indicates the measured area. (b) DOCT tomogram (4 mm × 2 mm). The arrows indicate the presence and position of the blood vessels (V_a and V_b). (c) Normalized time series of Doppler signal through the center of vessel V_a. Frequency analysis shows 0.15 Hz oscillation known as vaso-motion.

preparation. It has since been shown, by the same group, that this vaso-motion or V-signal also affects the levels of oxy- and deoxy-hemoglobin and so could be directly affecting the metabolism within the brain. The cause of the oscillation could be neurogenic[42] or myogenic[43] mechanisms.

Figure 6 illustrates a comparison of mechanical and flow dynamic changes during two instants of the V-signal cycle of the vessel V_a in Fig. 5(b). The time interval between the two images is ∼4.5 s, which, with reference to Fig. 5(c) corresponds to the first velocity peak and the following velocity

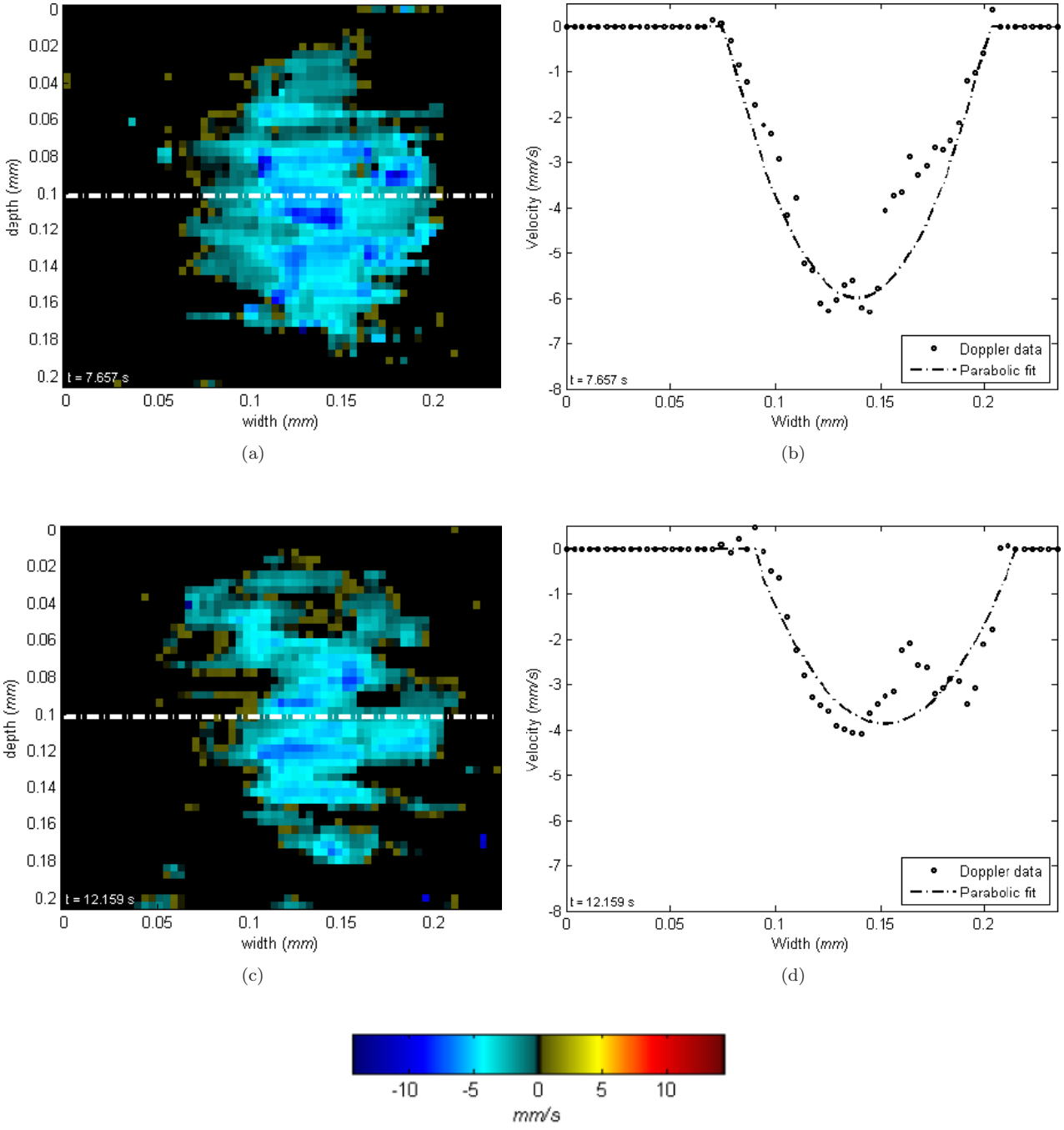

Fig. 6. *In vivo* cross-sectional subcranial arterial blood flow mapping at different time points during one V-signal cycle. (a) and (c) 2D Doppler data; the dashed line indicates the location where the single line blood flow velocity profile is observed. (b) and (d) are single line blood flow velocity profiles extracted from the 2D data at dashed line.

trough, respectively. To enhance the velocity data, the background, i.e. static tissue, has been subtracted. Figures 6(b) and 6(d) show a single line velocity profile extracted from the 2D data (dotted line). Data shows a variation of about 14.5% in the vessel diameter between the two images (from larger to smaller).

4. Discussion and Conclusions

SS-DOCT system has been applied for the investigation of feasibility studies on possible noninvasive determination of mechanical properties of blood microvessels. These pilot studies aimed to investigate the DOCT capability of indirectly monitoring

vessel compliance by simultaneous measurement of mechanical and flow dynamic changes of blood microvessels *in vivo*. The discrepancy between the measured (*in vitro* artificial vessel) and predicted pulse wave velocities unfortunately confounds attempts to relate this quantity to the underlying mechanical properties of the vessel. The most likely explanation for the discrepancy is that the equations quoted above are valid only for an infinitely long uniform elastic tube, where by definition wave reflections are absent. However, our model system contains a large mechanical impedance mismatch where the elastic tube meets the rigid outlet tube (see Fig. 1). It is well known that wave reflections can dramatically alter the apparent "input impedance" of the vascular system, which in turn means that the intravascular pressure associated with a given input volume flow rate can be radically altered. The vessel distension clearly reflects this pressure.

However, the preliminary results shown in this report demonstrate that DOCT can be potentially used for this purpose. From the acquired DOCT data it seems it is possible to determine vessel diameter (or perimeter) changes and related mean blood flow velocity. Further work is needed in the development of an artificial vessel whose shape and mechanical properties better match the ones of natural vessels, enabling a more accurate comparison of the experimental results (*in vitro* and *in vivo*) with the theoretical model. Further investigation and analysis is also needed for *in vivo* measurements. The vessel compliance is expressed as an indirect measure, function of instantaneous vessel radius, and mean blood flow cross-sectional velocity. It is therefore important to detect the vessel boundaries accurately from the DOCT data. The vessel boundaries could be estimated by setting a suitable threshold on the Doppler data; however, such methods have the disadvantage of cutting low values of the flow velocity, therefore introducing an error in vessel boundary detection using only the Doppler data. A cross-comparison between the structural data and the Doppler data is currently under investigation to evaluate eventual improvements in vessel boundary detection.

DOCT has a great potential for use in the clinical management of patients who can benefit from microvascular monitoring. Information provided by DOCT could be used to detect and diagnose atherosclerotic diseases; to monitor perfusion and viability before, during, and after reconstructive procedures; in the studies of the effects of blood flow dynamics in the artificial vessels and junctions used in cardiac by-pass surgery; or to screen human skin blood flow *in vivo*. Real-time DOCT imaging can monitor the transient flow behavior in human blood vessels due to the heartbeat and the non-Newtonian flow effects, with particular attention on the dependency of the blood viscosity on the local shear rate. Moreover, most of the cardiovascular studies rely on the computational fluid dynamics (CFD) results to determine the role and importance of that blood flow factors that could be involved in the genesis of cardiovascular diseases. DOCT, a tool capable of directly imaging the real physical situation, can assist CFD to significantly improve the quality of new therapeutic strategies or of already established interventional methods, as for example stent design and placement.

In conclusion, given the noninvasive nature of DOCT; the high spatial resolution; simple hardware requirement; and relatively compact size of the system, DOCT reveals itself as a potentially effective technique applicable in rheology and biomedicine, where noncontact, noninvasive, high resolution velocity mapping of moving constituents are of particular interest. In particular, neuroimaging applications could benefit from DOCT to investigate neuro-vascular coupling mechanisms, an area of current intense research.

Acknowledgments

This work has been made possible because of contribution from EPSRC Grant EP/E015077. The authors are also grateful to Thorlabs Ltd. UK for providing the swept source OCT system used in the *in vivo* experiments. We thank the laboratory technical staff in the Department of Psychology (Marion Simkins, Natalie Kennerley, and Malcolm Benn) for their assistance in the *in vivo* preparation.

References

1. S. R. Chinn, E. A. Swanson, "Optical coherence tomography for high-density data storage," in *Handbook of Optical Coherence Tomography*, B. E. Bouma, G. J. Tearney, Eds., Marcel Dekker Inc., New York (2002).
2. J. P. Dunkers, "Applications of optical coherence tomography to the study of polymer matrix composition," in *Handbook of Optical Coherence*

Tomography, B. E. Bouma, G. J. Tearney, Eds., Marcel Dekker Inc., New York (2002).
3. J. G. Fujimoto, M. E. Brezinski, G. J. Tearney, S. A. Boppart, M. R. Hee, E. A. Swanson, "Optical biopsy and imaging using optical coherence tomography," *Nat. Med.* **1**, 970–972 (1995).
4. D. Huang, E. A. Swanson, C. P. Lin, S. J. Schuman, W. G. Stinson, W. Chang, M. R. Hee, T. Flotte, K. Gregory, C. A. Puliafito, J. G. Fujimoto, "Optical coherence tomography," *Science* **254**, 1178–1181 (1991).
5. M. E. Brezinski, J. G. Fujimoto, "Optical coherence tomography: High resolution imaging in nontransparent tissue," *IEEE J. Sel. Topics Quant. Electr.* **5**, 1185–1192 (1999).
6. W. Drexler, "Ultrahigh-resolution optical coherence tomography," *J. Biomed. Opt.* **9**, 47–74 (2004).
7. B. E. Bouma, G. J. Tearney, *Handbook of Optical Coherence Tomography*, Marcel Dekker, Inc., New York (2002).
8. M. E. Brezinski, *Optical Coherence Tomography Principles and Applications*, Elsevier (2006).
9. A. F. Fercher, K. Mengedoht, W. Werner, "Eye-length measurement by interferometry with partially coherent light," *Opt. Lett.* **13**, 186–189 (1988).
10. E. A. Swanson, J. A. Izatt, R. Hee, D. Huang, C. P. Lin, S. J. Schuman, C. A. Puliafito, J. G. Fujimoto, "*In vivo* retinal imaging by optical coherence tomography," *Opt. Lett.* **18**(21), 1864–1866 (1993).
11. M. Wojtkowski, R. Leitgeb, A. Kowalczyk, T. Bajraszewski, A. F. Fercher, "*In vivo* human retinal imaging by Fourier domain optical coherence tomography," *J. Biomed. Opt.* **7**, 457–463 (2002).
12. R. Longmuir, G. L. Andrew, B. H. Culver, "Optical coherence tomography (OCT) in neuro-ophthalmology: A clinical perspective," *Neuro-Ophthalmology* **32**, 15–125 (2008).
13. J. M. Schmitt, D. Kolstad, C. Petersen, "Intravascular optical coherence tomography — opening a window into coronary artery disease Business briefing: European cardiology 2005," LightLab Imaging, Inc. (published online http://www.touchbriefings.com/pdf/1231/Lightlab_Tech.pdf) (2005).
14. X. Li, C. Chudoba, T. Ko, C. Pitris, J. G. Fujimoto, "Imaging needle for optical coherence tomography," *Opt. Lett.* **25**, 1520–1522 (2000).
15. J. H. Hwang, M. J. Cobb, M. B. Kimmey, X. Li, "Optical coherence tomography of the pancreas: A needle-based approach," *Clinic Gastroenterol. Hepatol.* **3**, S49–S52 (2005).
16. G. J. Tearney, H. Yabushita, S. L. Houser, H. T. Aretz, I.-K. Jang, K. H. Schlendorf, C. R. Kauffman, M. Shishkov, E. F. Halpern, B. E. Bouma, "Quantification of macrophage content in atherosclerotic plaques by optical coherence tomography," *Circulation* **107**, 113–119 (2003).
17. E. Regar, T. G. van Leeuwen, P. W. Serruys, *Optical Coherence Tomography in Cardiovascular Research*, Informa healthcare (2007).
18. N. A. Patel, D. L. Stamper, M. E. Brezinski, "Review of the ability of optical coherence tomography to characterize plaque, including a comparison with intravascular ultrasound," *Cardiovasc. Intervent. Radiol.* **28**, 1–9 (2005).
19. F. J. van der Meer, D. J. Faber, D. M. B. Sassoon, M. C. Aalders, G. Pasterkamp, T. G. van Leeuwen, "Localized measurement of optical attenuation coefficients of atherosclerotic plaque constituents by quantitative optical coherence tomography," *IEEE Trans. Med. Imaging* **24**, 1369–1376 (2005).
20. F. J. van der Meer, D. J. Faber, J. Perree, "Quantitative optical coherence tomography of arterial wall components," *Lasers Med. Sci.* **20**, 45–51 (2005).
21. J. A. Izatt, M. D. Kulkarni, S. Yazdanfar, J. K. Barton, A. J. Welch, "*In vivo* bidirectional colour Doppler flow imaging of picoliter blood volumes using optical coherence tomography," *Opt. Lett.* **22**, 1439–1441 (1997).
22. S. Yazdanafar, M. D. Kulkarni, J. A. Izatt, "High resolution imaging of *in vivo* cardiac dynamics using colour Doppler optical coherence tomography," *Opt. Exp.* **1**, 424–431 (1997).
23. S. Yazdanafar, A. M. Rollins, J. A. Izatt, "*In vivo* imaging of human retinal flow dynamics by colour Doppler optical coherence tomography," *Arch. Ophthalmol.* **121**, 235–239 (2003).
24. Z. Chen, T. E. Milner, S. Srinivas, X. Wang, A. Malekafzali, J. C. van Gemert, J. S. Nelson, "Noninvasive imaging of *in vivo* blood flow velocity using optical Doppler tomography," *Opt. Lett.* **22**, 1119–1121 (1997).
25. J. K. Barton, J. A. Izatt, M. D. Kulkarni, S. Yasdanfar, A. J. Welch, "Three-dimensional reconstruction of blood vessels from *in vivo* colour Doppler optical coherence tomography images," *Dermatology* **198**, 355–361 (1999).
26. M. Bonesi, D. Churmakov, I. Meglinski, "Study of flow dynamics in complex vessels using Doppler optical coherence tomography," *Meas. Sci. Technol.* **18**, 3279–3286 (2007).
27. M. Bonesi, D. Churmakov, L. J. Ritchie, I. V. Meglinski, "Optical coherence tomography imaging depth enhancement by superficial skin optical clearing," *Laser Phys. Lett.* **4**, 304–307 (2006).
28. T. G. van Leeuwen, M. D. Kulkarni, S. Yazdanfar, A. M. Rollins, J. A. Izatt, "High-flow-velocity and shear-rate imaging by use of color Doppler optical coherence tomography," *Opt. Lett.* **24**, 1584–1586 (1999).
29. J. Moger, S. J. Matcher, C. P. Winlove, A. Shore, "Measuring red blood cell flow dynamics in a glass capillary using Doppler optical coherence

tomography and Doppler amplitude optical coherence tomography," *J. Biomed. Opt.* **9**, 982–994 (2004).
30. A. M. Rollins, S. Yazdanfar, J. K. Barton, J. A. Izatt, "Real-time *in vivo* colour Doppler optical coherence tomography," *J. Biomed. Opt.* **7**, 123–129 (2002).
31. C. J. Chang, K. H. Hou, "High-resolution optical Doppler tomography for *in vitro* and *in vivo* fluid flow dynamics," *Chang Gung Med. J.* **26**, 403–411 (2003).
32. Y. Satomura, J. Seki, Y. Ooi, T. Yanagida, A. Seiyama, "*In vivo* imaging of the rat cerebral microvessels with optical coherence tomography," *Clin. Hemorheol. Microcir.* **31**, 31–40 (2004).
33. S. G. Proskurin, I. V. Meglinski, "Optical coherence tomography imaging depth enhancement by superficial skin optical clearing," *Laser Phys. Lett.* **4**, 824–826 (2007).
34. M. C. Pierce, J. Strasswimmer, B. Hyle Park, B. Cense, J. F. de Boer, "Advances in optical coherence tomography imaging for dermatology," *J. Invest. Dermatol.* **123**, 458–463 (2004).
35. T. Gambichler, G. Moussa, M. Sand, D. Sand, P. Altmeyer, K. Hoffmann, "Applications of optical coherence tomography in dermatology," *J. Dermatol. Sci.* **40**, 85–94 (2005).
36. M. Born, E. Wolf, *Principles of Optics: Electromagnetic Theory of Propagation, Interference and Diffraction of Light*, Cambridge University Press, Cambridge, UK (1999).
37. A. F. Fercher, W. Drexler, C. K. Hitzenberger, T. Lasser, "Optical coherence tomography — principles and applications, *Rep. Prog. Phys.* **66**, 239–303 (2003).
38. V. V. Tuchin, *Handbook of Coherent Domain Optical Methods*, Kluwer Academic Press (2004).
39. W. Drexler, J. G. Fujimoto, Eds., *Optical Coherence Tomography*, Springer (2008).
40. A. G. Udetz, R. J. Roman, D. R. Harder, "Spontaneous flow oscillations in the cerebral cortex during acute changes in mean arterial pressure," *J. Cereb. Blood Flow Metabol.* **12**, 491–499 (1992).
41. J. E. Mayhew, S. Askew, Y. Zheng, J. Porrill, G. W. M. Westby, P. Redgrave, D. M. Rector, R. M. Harper, "Cerebral vasomotion: 0.1 Hz oscillation in reflected light imaging neural activity," *Neuroimage* **4**, 183–193 (1996).
42. E. V. Golanov, D. Reis, "Vasodilatation evoked from medulla and cerebellum is coupled to bursts of cortical EEG activity in rats," *Am. J. Physiol.* **268**, R454–467 (1995).
43. B. Folkow, "Description of the myogenic hypothesis," *Circ. Res.* **20**, 327–335 (1964).